Kobe J. Med. Sci., Vol. 63, No. 3, pp. E84-E91, 2017

Evaluation of a Small Animal Irradiation System for Animal Experiments Using EBT3 Model GAFCHROMIC^{TM} Film

YASUYUKI SHIMIZU[1], HIROAKI AKASAKA[2], DAISUKE MIYAWAKI[1,2], NARITOSHI MUKUMOTO[2], MASAO NAKAYAMA[3], TIANYUAN WANG[1], SAKI OSUGA[1], SACHIKO INUBUSHI[1], RYUICHI YADA[1], YASUO EJIMA[2], KENJI YOSHIDA[1,2], TAKEAKI ISHIHARA[1,2], and RYOHEI SASAKI[1,2*]

[1] *Division of Radiation Oncology, Kobe University Graduate School of Medicine, 7-5-2 Kusunokicho, Chuo-ku, Kobe, Hyogo, 650-0017, Japan*

[2] *Division of Radiation Oncology, Kobe University Hospital, 7-5-2 Kusunokicho, Chuo-ku, Kobe, Hyogo, 650-0017, Japan*

[3] *Division of Radiation Oncology, Kobe Minimally Invasive Cancer Center, 8-5-1, Minatojima-nakamachi, Chuo-ku, Kobe, Hyogo, 650-0046, Japan*

[*] *Corresponding author*

Received 3 August 2017/ Accepted 4 September 2017

Key words: Radiation, Animal experiment, Quality assurance, Irradiation.

In cancer research, small animal models, for example, mice, rats, or rabbits, facilitate the in-depth study of biological processes and the effects of radiation treatment that can lead to breakthrough discoveries. However, the physical quality of small animal irradiation systems has not been previously evaluated. In this study, we evaluate the quality of a small animal irradiation system using GAFCHROMIC^{TM} film and a Tough Water Phantom. The profiles and percentage depth dose curves for several irradiation conditions were measured to evaluate the quality of the irradiation system. The symmetry ratios when the table was rotated were 1.1 (no filter), 1.0 (0.5 mm Al filter), 1.0 (1.0 mm Al filter), 1.1 (2 mm Al filter), and 1.0 (filter consisting of 0.5 mm Al combined with 0.1 mm Cu). The results of measuring the percentage depth dose curve showed that the relative doses were 17.5% (10 mm depth), 12.4% (20 mm depth), 9.5% (30 mm depth), and 7.4% (40 mm filter) with no filters inserted, 78.0% (10 mm depth), 61.1% (20 mm depth), 46.9% (30 mm depth), and 35.3% (40 mm depth) when a 1.0 mm Al filter was inserted, and 94.4% (10 mm depth), 81.7% (20 mm depth), 68.1% (30 mm depth), and 54.7% (40 mm depth) when a filter consisting of 1.0 mm Al combined with 0.2 mm Cu was inserted. These physical assessments seem to be necessary especially in vivo experiments because those increase reliability of data obtained from small animal irradiation systems.

INTRODUCTION

Radiotherapy using X-rays is one of the most commonly used therapeutic modalities in cancer treatment. The benefit of using X-rays is that they are a type of ionizing radiation that exhibits both wave-like and particle-like properties, and can ionize the H_2O molecules of tumor cells and cause damage to their DNA [1]. However, these effects are not limited to tumor cells, but can also affect normal cells within the tumor stroma [2–3]. The cytotoxicity of radiation is mostly mediated through the generation of DNA double-strand breaks (DSBs), as demonstrated by the radiosensitivity of defective cells and organisms in the machinery of DSB repair [4–6].

In general, the high energy (megavoltage) radiation systems that are used clinically are of high quality and stable. In contrast, the physical quality of low energy radiation machines has not been evaluated. At our institution, low energy radiation machines have been primarily used for *in vitro* and *in vivo* studies [7–18]. To apply those experimental results to clinical applications, it is essential that the physical quality of the radiation machines be evaluated. From this point of view, we assessed the physical quality of a radiation system that used EBT3 model GAFCHROMIC^{TM} film, which was the first type of radiochromic film that was suitable for use with radiation doses [19]. We expect that this report will be useful for either researchers who will use the irradiation system at the Kobe University, or those who use similar irradiation system at other institutions because the results of the physical assessment of the radiation machine will provide confidence regarding the effects of the radiation.

Phone: +81-78-3825687, Fax: +81-78-3826734, E-mail: rsasaki@med.kobe-u.ac.jp

MATERIALS AND METHODS

Radiochromic film

In this study, EBT3 model GAFCHROMIC^{TM} film (Lot # 09151402, International Specialty Products Inc., Wayne, NJ, USA) was used. The substrate of this film is matte polyester (125 µm thick) coated with an active layer (28 µm thick) over which the matte polyester laminate (125 µm thick) is applied. The active layer contains a yellow dye, which is referred to by the manufacturer as a marker dye, and is added to correct for subtle differences in the thickness of the active layer. In addition to being symmetric, EBT3 model GAFCHROMIC^{TM} film features anti-Newton ring particles, which are embedded silica particles within protective polyester layers.

Calibration of the film measurement was performed using a scanner (ES-10000G, Epson, Tokyo, Japan) according to the protocol described by Devic et al. [20]. Each film was irradiated 24 h before being scanned using a 48-bit RGB mode.

Radiation machine

Irradiation was performed using an MBR-1505R2 X-ray generator (Hitachi Medical Co., Tokyo, Japan) at a voltage of 150 kV and current of 5 mA, which delivered a dose rate of 0.8 Gy/min. The radiation machine system contains detachable metal filters (0.5 mm, 1.0 mm, and 2.0 mm aluminum (Al) filters, and a 0.1 mm copper (Cu) filter) to adjust the irradiated energy.

Physical assessment of the radiation machine

The exit field size of the X-ray generator was 5 cm in diameter, and the beam profiles were measured along the transverse and longitudinal axes with and without turn table rotation, as shown in Fig. 1a. To obtain the beam profiles of the radiation machine, the EBT3 model GAFCHROMIC^{TM} films were set on the surface of a Tough Water Phantom (TWP) WD-4005 and WD-4010 (Kyoto Kagaku Co., LTD, Japan) with a source-to-surface distance (SSD) setup of 250, 400, and 550 mm (each field size on the turn table was 160, 260, and 360 mm, respectively). For the percentage depth dose (PDD) curve measurement, the EBT3 model GAFCHROMIC^{TM} films were positioned at the beam axis within the TWP. The EBT3 model GAFCHROMIC^{TM} films were set at depths of 5, 10, 15, 20, 30, and 40 mm in the TWP, and were irradiated without rotation (Fig. 1b).

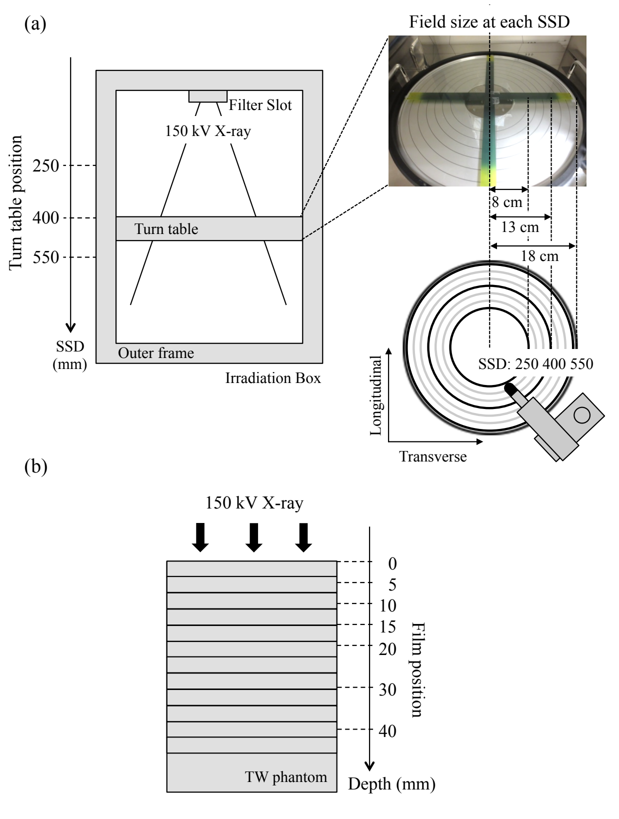

Figure 1. (a) Schematic of the irradiation system used in this study, and the experimental setup used for the profile measurements. (b) Experimental setup for the PDD curve measurements.

Calibration curve

Irradiation was performed to obtain the calibration curve. In a 13-cm diameter field size, films were placed at the surface on the TWP at an SSD of 300 mm. Ion chamber measurements were used to determine the dose delivered by the x-ray beam at the same depths on the TWP. The TWP was constructed from 25 x 25 cm^2 plates, and the films were set between those plates. The EBT3 film calibration curves were determined by means of eight film pieces irradiated by 0 to 20 Gy absorbed doses to the water. An EPSON ES-10000G color scanner was used to analyze the film in transmission mode. The scanner response stability, intrafilm uniformity, and interfilm reproducibility were selected by adjusting the scanning parameters. The optical absorption spectra measurements were conducted using both non-irradiated and irradiated EBT3 films to determine the most sensitive color windows within the radiation dose ranges used.

Evaluation of the dose distribution in the *in vivo* experimental setting

The dose distribution was measured by exposing the EBT3 film to 15 Gy of irradiation with a 1 mm Al filter. Mice were anesthetized by the intraperitoneal administration of somnopentyl (0.1 mg/g body weight) and were positioned face up. Then, EBT3 films were placed on the anterior or posterior sides of the mice. Four mice were placed side-by-side, and the SSD was set to 400 mm. After 24 h, the irradiated films were scanned and analyzed with the ImageJ 1.48 v software (National Institutes of Health, Bethesda, MD, USA). This study was approved by the Institutional Animal Care and Use Committee (Permission number: P120606-R2) and carried out according to the Kobe University Animal Experimentation Regulation.

Analysis

The symmetries of each profile were calculated using the following equation:

–The maximum dose ratio = $(D_x/D_{-x})_{max}$

where D_x and D_{-x} are the dose at the x and $-x$ positions, respectively, which are symmetric relative to the central axis [21].

RESULTS

Profile measurements

The profiles without turn table rotation are shown in Figs. 2a and 2b, and those with turn table rotation are shown in Fig. 2c. The symmetry of each profile is listed in Table I. Without turn table rotation, the profiles along the longitudinal axis (symmetry: 1.99 ± 0.94) were more symmetric than those along the transverse axis (symmetry: 1.03 ± 0.008). In contrast, with turn table rotation, the symmetry improved remarkably (symmetry without rotation: 1.99 ± 0.94, symmetry with rotation: 1.05 ± 0.02). The profiles at 250, 400, and 550 mm SSD settings with a 1 mm Al filter are shown in Fig. 3.

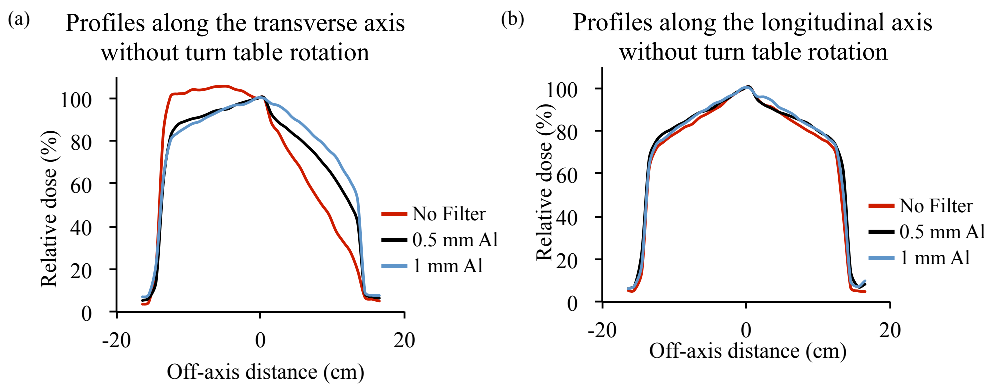

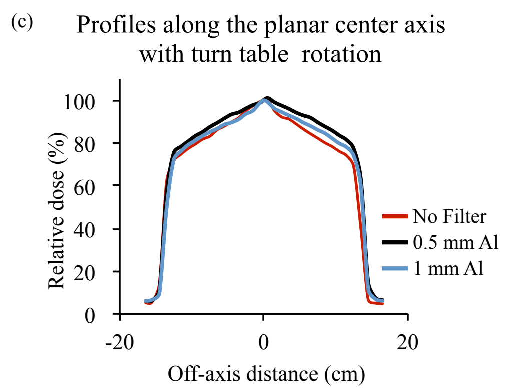

Figure 2. Radiation beam profiles obtained with several filter settings. (a) Profiles along the transverse axis without rotation. (b) Profiles along the longitude axis without rotation. (c) Profiles with rotation.

Table I. The symmetry of each beam profiles at SSD 400 mm. The ratio of each beam profiles to ideal profiles.

	Filters									
	No filter		Al 0.5 mm		Al 1.0 mm		Al 2.0 mm		Al 0.5 mm + Cu 0.1 mm	
Rotation	transverse	longitudinal	transverse	longitudinal	transverse	longitudinal	transverse	longitudinal	transverse	longitudinal
(−)	3.60	1.02	2.00	1.03	1.64	1.02	1.38	1.03	1.31	1.04
(+)	1.08		1.04		1.03		1.06		1.03	

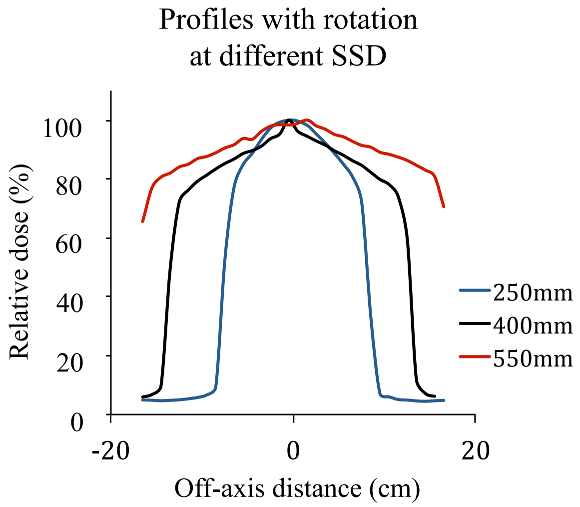

Figure 3. The profiles with turn table rotation at 250 mm, 400 mm, or 550 mm SSD setting.

Percentage depth dose curves

Figure 4 showed the PDD curves with or without each filter. Without the filters, the relative doses at depths of 10, 20, 30, and 40 mm were 17.5%, 12.4%, 9.5%, and 7.4%, respectively. With the 1 mm Al filter, the relative doses at the same depth were 78%, 61.1%, 46.9%, and 35.3%, respectively. With the combined 1 mm Al and 0.2 mm Cu filters, the relative doses were 94.4%, 81.7%, 68.1%, and 54.7%, respectively.

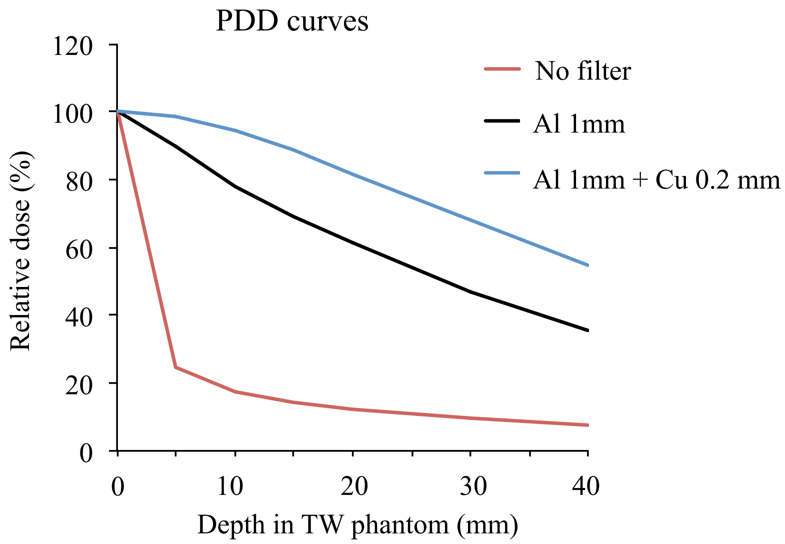

Figure 4. Several PDD curves with several filters inserted without the turn table rotating.

Evaluation of the dose distribution in an *in vivo* experimental setting

The calibration curve and measurement of the dose distributions using the films are shown in Figs. 5a-b. The calculated absolute doses are shown in Table II. With a 1 mm Al filter, the doses to the front of the abdominal skin of the mice were 1.68 – 1.89 times higher than those to the back surface. The position of the mice (inner or outer) seemed to affect the distribution of the doses.

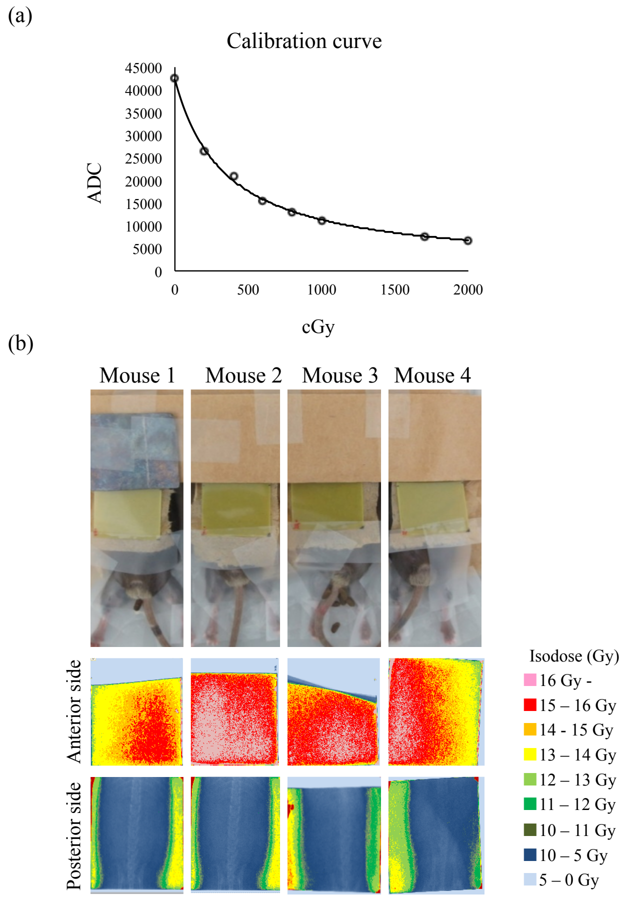

Figure 5. Absolute dose and dose distribution measurements. (a) Calibration curve of the EBT3 film used in this study. (b) The dose distribution that was obtained from the EBT3 films at the anterior or posterior sides of the mice.

Table II. The absolute dose of the skin of mouse

Film position	Dose (Gy)			
	Mouse 1	Mouse 2	Mouse 3	Mouse 4
Anterior side	14.67	15.86	15.59	14.96
Posterior side	8.62	8.38	8.87	8.92
Dose ratio	1.7	1.89	1.76	1.68

DISCUSSION

In the present study, we found that the beam profile had better homogeneity when the table was rotating versus when it was stopped. In addition, our results suggested that the choice of filter affected the depth dose profile in the body of the animal; consequently, we recommend researchers carefully select an appropriate filter that matches the settings of each experiment.

In general, researchers use small animal irradiation systems without performing individual quality checks of the system. Until now, there have been few reports about the physical evaluation of small animal irradiation systems [22]. Mesbahi A *et al.* reported on the beam spectral characteristics using a Monte Carlo simulation. However, there is uncertainty about the beam profile of the entire irradiation field used in this study because the authors did not provide the results of beam profile measurements obtained using a film detector. In present study, all measurements were performed using a film detector to investigate the beam profile and depth dose curve of the entire irradiation field.

For profile measurements, the profiles when the turn table was rotating exhibited better symmetry than when the turn table was stopped. In addition, when the turn table was stopped, the profiles along the longitudinal axis exhibited better symmetry than the profiles along the transverse axis. In this study, the transverse axis runs in a direction parallel to the anode-cathode axis. The heel effect is more pronounced in the transverse direction, and the heel effect has a direct influence on the profiles. Due to the heel effect, the beam was seen to decrease by about 60% on the anode side of the field [23].

For PDD measurements, these results indicated that the "no filter" setting was suitable for shallow targets, such as skin, although filter settings were identified that were suitable for deep targets, such as the abdomen. In addition, the combination of a 1 mm Al filter and a 0.2 mm Cu filter exhibited the most uniform depth dose distribution in this study. In general, the body thickness of a mouse or rat is about 2 mm or 4 mm, respectively. Our results suggest that the combined 1 mm Al and 0.2 mm Cu filters provided better coverage for the body thickness of small animals than that of the other filters.

The measurement results of the dose distribution from the film indicated that the mouse should be placed near the center of the irradiation field. The absolute dose of a mouse that was placed at the edge of the irradiation field was 0.63 – 1.19 Gy lower than that of mouse placed near center of the irradiation field. Researchers should note the decreased irradiation dose near the edges to avoid misunderstanding their results. For these reasons, the position of a mouse in the X-ray generator and the appropriate radiation exit filter should be selected carefully, depending on the requirements of each experiment.

When this x-ray generator was used for *in vitro* experiments, some researchers inserted several filters on the exit of the x-ray generator, while others did not insert any filters. Thus, the combinations of filters used in their reports vary widely depending on the intended use: no filter [24-32], a 1 mm Al filter combined with 0.2 mm Cu filter [33-35], a 1 mm Al filter [17, 36-39], a 0.5 mm Al filter combined with a 1 mm Cu filter [40], or a 1 mm Al filter combined with a 0.5 mm Cu filter [41]. For the *in vivo* experiments, the filters used in each report also vary widely: no filter [25, 42-45], a 1 mm Al filter [17, 36-37, 39], a 0.2 mm Al filter combined with a 0.5 mm Cu filter [46], a 0.5 mm Al filter [47], or a 2 mm Al filter [48]. If the depth of the irradiated cells in the dishes were shallow *in vitro* experiments, and the tumors were located below the skin, any combination of filters could be selected. Although, if the tumor was seated deeply in the body, it was also possible to use no filters.

In conclusion, small animal irradiation systems should be used with the turn table rotating. We anticipate that this report will prove to be an important reference document for all researchers who plan to use this small animal irradiation system henceforth, as it shows how to obtain the most reliable results.

ACKNOWLEDGEMENTS

This work was supported by Grants-in-Aid (nos. 16K15581 and 16H05391 to RS and no. 16K19818 to NM) for Exploratory Research from the Ministry of Education, Culture, Sports, Science, and Technology of Japan.

REFERENCES

1. **Haimovitz-Friedman, A.** 1998. Radiation-induced signal transduction and stress response. Radiat Res **150:** 102–108.
2. **Garcia-Barros, M., Paris, F., Cordon-Cardo, C., Lyden, D., Rafii, S., Haimovitz-Friedman, A., Fuks, Z., and Kolesnick, R.** 2003. Tumor response to radiotherapy regulated by endothelial cell apoptosis. Science **300**: 1155–1159.
3. **Paris, F., Fuks, Z., Kang, A., Capodieci, P., Juan, G., Ehleiter, D., Haimovitz-Friedman, A., Cordon-Cardo, C., and Kolesnick, R.** 2001. Endothelial apoptosis as the primary lesion initiating intestinal radiation damage in mice. Science **293**: 293–297.
4. **Li, Y., Carty, M.P., Oakley, G.G., Seidman, M.M., Medvedovic, M., and Dixon, K.** 2001. Expression of ATM in ataxia telangiectasia fibroblasts rescues defects in DNA double-strand break repair in nuclear extracts. Environ Mol Mutagen **37**: 128–140.
5. **El-Awady, R.A., Dikomey, E., and Dahm-Daphi, J.** 2003. Radiosensitivity of human tumor cells are correlated with the induction but not with the repair of DNA double-strand breaks. Br J Cancer **89**: 593–601.
6. **Sakata, K., Someya, M., Matsumoto, Y., and Hareyama, M.** 2007. Ability to repair DNA double-strand breaks related to cancer susceptibility and radiosensitivity. Radiat Med **25**: 433–438.
7. **Onishi, Y., Akisue, T., Kawamoto, T., Ueha, T., Hara, H., Toda, M., Harada, R., Minoda, M., Morishita, M., and Sasaki, R.** 2014. Transcutaneous application of CO2 enhances the antitumor effect of radiation therapy in human malignant fibrous histiocytoma. Int J Oncol **45**(2): 732–738.
8. **Mukubou, H., Tsujimura, T., Sasaki, R., and Ku, Y.** 2010. The role of autophagy in the treatment of pancreatic cancer with gemcitabine and ionizing radiation. Int J Oncol **37**(4): 821–828.
9. **Zhang, Z., Shirakawa, T., Hinata, N., Matsumoto, A., Fujisawa, M., Okada, H., Kamidono, S., Matsuo, M., and Gotoh, A.** 2003. Combination with CD/5-FC gene therapy enhances killing of human bladder-cancer cells by radiation. J Gene Med **5**(10): 860–867.
10. **Tsujino, K., Kodama, A., Kanaoka, N., Maruta, T., and Kono, M.** 1999. Expression of pulmonary mRNA encoding ICAM-1, VCAM-1, and P-selectin following thoracic irradiation in mice. Radiat Med **17**(4): 283–287.

11. **Matsumoto, A., Matsumoto, R., Enomoto, T., and Itoh, K.** 1998. A human brain proteolytic activity capable of cleaving natural beta-amyloid precursor protein is affected by its substrate glycoconjugates. Neurosci Lett **242**(2): 109–113.
12. **Uchida, T., Kitaura, J., Nakahara, F., Togami, K., Inoue, D., Maehara, A., Nishimura, K., Kawabata, K.C., Doki, N., Kakihana, K., Yoshioka, K., Izawa, K., Oki, T., Sada, A., Harada, Y., Ohashi, K., Katayama, Y., Matsui, T., Harada, H., and Kitamura, T.** 2014. Hes1 upregulation contributes to the development of FIP1L1-PDGRA-positive leukemia in blast crisis. Exp Hematol **42**(5): 369–379.
13. **Nakahara, F., Sakata-Yanagimoto, M., Komeno, Y., Kato, N., Uchida, T., Haraguchi, K., Kumano, K., Harada, Y., Harada, H., Kitaura, J., Ogawa, S., Kurokawa, M., Kitamura, T., and Chiba, S.** 2010. Hes1 immortalizes committed progenitors and plays a role in blast crisis transition in chronic myelogenous leukemia. Blood **115**(14): 2872–2881.
14. **Kagiyama, Y., Kitaura, J., Togami, K., Uchida, T., Inoue, D., Matsukawa, T., Izawa, K., Kawabata, K.C., Komeno, Y., Oki, T., Nakahara, F., Sato, K., Aburatani, H., and Kitamura, T.** 2012. Upregulation of CD200R1 in lineage-negative leukemic cells is characteristic of AML1-ETO-positive leukemia in mice. Int J Hematol 96(5): 638–648.
15. **Watanabe-Okochi, N., Kitaura, J., Ono, R., Harada, H., Harada, Y., Komeno, Y., Nakajima, H., Nosaka, T., Inaba, T., and Kitamura, T.** 2008. AML1 mutations induced MDS and MDS/AML in a mouse BMT model. Blood 111(8): 4297–4308.
16. **Kato, N., Kitaura, J., Doki, N., Komeno, Y., Watanabe-Okochi, N., Togami, K., Nakahara, F., Oki, T., Enomoto, Y., Fukuchi, Y., Nakajima, H., Harada, Y., Harada, H., and Kitamura, T.** 2011. Two types of C/EBP α mutations play distinct but collaborative roles in leukemogenesis: lessons from clinical data and BMT models. Blood 117(1): 221–233.
17. **Nakayama, M., Sasaki, R., Ogino, C., Tanaka, T., Morita, K., Umetsu, M., Ohara, S., Tan, Z., Nishimura, Y., Akasaka, H., Sato, K., Numako, C., Takami, S., and Kondo, A.** 2016. Titanium peroxide nanoparticles enhanced cytotoxic effects of X-ray irradiation against pancreatic cancer model through reactive oxygen species generation *in vitro* and *in vivo*. Radiat Oncol **11**(1): 91.
18. **Akasaka, H., Mizushina, Y., Yoshida, K., Ejima, Y., Mukumoto, N., Wang, T., Inubushi, S., Nakayama, M., Wakahara, Y., and Sasaki, R.** 2016. MGDG extracted from spinach enhances the cytotoxicity of radiation in pancreatic cancer cells. Radiat Oncol **11**(1): 153, 2016
19. **Casanova Borca, V., Pasquino, M., Russo, G., Grosso, P., Cante, D., Sciacero, P., Girelli, G., La Porta, M.R., and Tofani, S.** 2013. Dosimetric characterization and use of GAFCHROMIC EBT3 film for IMRT dose verification. J Appl Clin Med Phys **14**(2):4111. doi: 10.1120/jacmp.v14i2.4111.
20. **Devic, S., Seuntjens, J., Sham, E., Podgorsak, E.B., Schmidtlein, C.R., Kirov, A.S., and Soares, C.G.** 2005. Precise radiochromic film dosimetry using a flat-bed document scanner. Med Phys **32**(7): 2245–2253.
21. **Fogliata, A., Garcia, R., Knoos, T., Nicolini, G., Clivio, A., Vanetti, E., Khamphan, C., and Cozzi, L.** 2012. Definition of parameters for quality assurance of flattening filter free (FFF) photon beams in radiation therapy. Med Phys **39**(10): 6455–6464.
22. **Mesbahi, A. and Zakariaee, S.S.** 2013. Effect of anode angle on photon beam spectra and depth dose characteristics for X-RAD320 orthovoltage unit. Rep Pract Oncol Radiother **18**(3): 148–152.
23. **Rana, V., Gill, K., Rudin, S., and Bednarek, D.R.** 2012. Significance of including field non-uniformities such as the heel effect and beam scatter in the determination of the skin dose distribution during interventional fluoroscopic procedures. Proc SPIE Int Soc Opt Eng **23**: 8313.
24. **Goda, N., Yamamoto, Y., Nakamura, T., Kusuhara, T., and Maruyama, T.** 2007. Quantitative evaluation of micromotion of cultured cells using electrical cell-substrate impedance sensing (EelS) method cell-to-cell distance and cell-to-substrate distance. Bull Fac Health Sci **17**: 9–15.
25. **Tsukamoto, H., Shibata, K., Kajiyama, H., Terauchi, M., Nawa, A., and Kikkawa, F.** 2008. Aminopeptidase N (APN)/CD13 inhibitor, Ubenimex, enhances radiation sensitivity in human cervical cancer. BMC Cancer **8**(74).
26. **Nakajima, A., Nishimura, K., Nakaima, Y., Oh, T., Noguchi, S., Taniguchi, T., and Tamura, T.** 2009. Cell type-dependent proapoptotic role of Bcl2L12 revealed by a mutation concomitant with the disruption of the juxtaposed Irf3 gene. PNAS **106**(30): 12448–12452.
27. **Ookawa, K., Kudo, T., Aizawa, S., Saito, H., and Tsuchida, S.** 2002. Transcriptional activation of the MUC2 gene by p53. J Biol Chem 277(50): 48270–48275.
28. **Sato, K., Yamashita, N., Baba, M., and Matsuyama, T.** 2003. Modified myeloid dendritic cells act as regulatory dendritic cells to induce anergic and regulatory T cells. Blood **101**(9): 3581–3589.
29. **Kiyozuka, M., Akimoto, T., Fukutome, M., Motegi, A., and Mitsuhashi, N.** 2013. Radiation-induced dimer formation of EGFR: Implications for the radiosensitizing effect of Cetuximeb. Anticancer Res 33:

4337–4346.

30. **Wu, X., Liu, W., Cao, Q., Chen, C., Chen, Z., Xu, Z., Li, W., Liu, F., and Yao, X.** 2014. Inhibition of Aurora B by CCT137690 sensitizes colorectal cells to radiotherapy. J Exp Clin Cancer Res **33**: 13.
31. **Uchida, D., Begum, N-M., Almofti, A., Kawamata, H., Yoshida, H., and Sato, M.** 2004. Frequent downregulation of 14-3-3 s protein and hypermethylation of 14-3-3 s gene in salivary gland adenoid cystic carcinoma. Br J Cancer **91**: 1131–1138.
32. **Kazuki, Y., Hoshiya, H., Kai, Y., Abe, S., Takiguchi, M., Osaki, M., Kawazoe, S., Katoh, M., Kanatsu-Shinohara, M., Inoue, K., Kajitani, N., Yoshino, T., Shirayoshi, Y., Ogura, A., Shinohara, T., Barrett, J.C., and Oshimura, M.** 2008. Correction of a genetic defect in multipotent germline stem cells using a human artificial chromosome, Gene Therapy **15**: 617–624.
33. **Koana, T. and Tsujimura, H.** 2010. A u-shaped dose–response relationship between X-radiation and sex-linked recessive lethal mutation in male germ cells of Drosophila. Radiat Res **174**: 46–51.
34. **Hoshi, Y., Tanooka, H., Miyazaki, K., and Wakasugi, H.** 1997. Induction of thioredoxin in human lymphocytes with low-dose ionizing radiation. Biochimica et Biophysica Acta **1359**: 65–70.
35. **Koana, T., Okada, M.O., Ogura, K., Tsujimura, H., and Sakai, K.** 2007. Reduction of background mutations by low-dose X-irradiation of Drosophila Spermatocytes at a low dose rate. Radiat Res **167**: 217–221.
36. **Harada, T., Harada, K., and Ueyama, Y.** 2012. The enhancement of tumor radio response by combined treatment with cepharanthine is accompanied by the inhibition of DNA damage repair and the induction of apoptosis in oral squamous cell carcinoma. Int J Oncol **41**: 565–572.
37. **Harada, K., Ferdous, T., Cui, D., Kuramitsu, Y., Matsumoto, T., Ikeda, E., Okano, H., and Ueyama, Y.** 2016. Induction of artificial cancer stem cells from tongue cancer cells by defined reprogramming factors. BMC Cancer **16**: 548.
38. **Watanabe, N., Yokoyama, K., Kinuya, S., Shuke, N., Shimizu, M., Michigishi, T., Tonami, N., Seto, H., and Goodwin, D.A.** 1998. Radiotoxicity after Strontium-89 therapy for bone metastases using the micronucleus assay. J Nucl Med **39**(12): 2077-2079.
39. **Akasaka, H., Mizushina, Y., Yoshida, K., Ejima, Y., Mukumoto, N., Wang, T., Inubushi, S., Nakayama, M., Wakahara, Y., and Sasaki, R.** 2016. MGDG extracted from spinach enhances the cytotoxicity of radiation in pancreatic cancer cells. Radiat Oncol **11**: 153.
40. **Oita, M., Uto, Y., Tominaga, M., Sasaki, M., Hara, Y., Kishi, T., and Hitoshi, H.** 2014. Radiosensitivity uncertainty evaluation for the *in vitro* biophysical modeling of EMT6 Cells. Anticancer Res **34**: 4621-4626.
41. **Shimura, T., Hamada, N., Sasatani, M., Kamiya, K., and Kunugita, N.** 2014. Nuclear accumulation of cyclin D1 following long-term fractionated exposures to low-dose ionizing radiation in normal human diploid cells. Cell Cycle **13**(8): 1248–1255.
42. **Yasuda, K., Nirei, T., Tsuno, N.H., Nagawa, H., and Kitayama, J.** 2011. Intratumoral injection of interleukin-2 augments the local and abscopal effects of radiotherapy in murine rectal cancer. Cancer Sci **102**(7): 1257–1263.
43. **Shibata, T., Nagata, K., and Kobayashi, Y.** 2007. Cutting Edge: A critical role of nitrogen oxide in preventing inflammation upon apoptotic cell clearance. J Immunol **179**: 3407–3411.
44. **Wang, C., Abe, S., Matsuda, K., Yu, C., Li, Y., Usuki, J., Azuma, A., and Kudoh, S.** 2008. Effects of Gefitinib on radiation-induced lung injury in mice. J Nippon Med Sch **75**(2): 96–105.
45. **Miura, T., Mizuki, D., Sasaki, S., Hasegawa, S., Sashinami, H., and Nakane, A.** 2000. Host resistance to Listeria monocytogenes infection is enhanced but resistance to Staphylococcus aureus infection is reduced in acute graft-versus-host disease in mice. Infect Immun **68**(7): 4340–4343.
46. **Kataoka, T., Yoshimoto, M., Nakagawa, S., Mizuguchi, Y., Taguchi, T., and Yamaoka, K.** 2009. Basic study on active changes in biological function of mouse liver graft in cold storage after low-dose X-irradiation. J Clin Biochem Nutr **45**: 219–226.
47. **Watanabe, S., Fujita, M., Ishihara, M., Tachibana, S., Yamamoto, Y., Kaji, T., Kawauchi, T., and Kanatani, Y.** 2014. Protective effect of inhalation of hydrogen gas on radiation-induced dermatitis and skin injury in rats. J Radiat Res **55**: 1107–1113.
48. **Sato, T., Kinoshita, M., Yamamoto, T., Ito, M., Nishida, T., Takeuchi, M., Saitoh, D., Seki, S., and Mukai, Y.** 2015. Treatment of irradiated mice with high-dose ascorbic acid reduced lethality. PLOS One **10**(2): e0117020.